

Spin-waves in antiferromagnetic single-crystal LiFePO_4

Jiyang Li,* Vasile O. Garlea, Jerel L. Zarestky, and David Vaknin†

Ames Laboratory and Department of Physics and Astronomy, Iowa State University, Ames, Iowa 50011, USA

(Received 19 August 2005; revised manuscript received 18 October 2005; published 18 January 2006)

Spin-wave dispersions in the antiferromagnetic state of single-crystal LiFePO_4 were determined by inelastic neutron scattering measurements. The dispersion curves measured from the (0,1,0) reflection along both a^* and b^* reciprocal-space directions reflect the anisotropic coupling of the layered Fe^{2+} ($S=2$) spin system. The spin-wave dispersion curves were theoretically modeled using linear spin-wave theory by including in the spin Hamiltonian in-plane nearest- and next-nearest-neighbor interactions (J_1 and J_2), inter-plane nearest-neighbor interactions (J_\perp) and a single-ion anisotropy (D). A weak (0,1,0) magnetic peak was observed in elastic neutron scattering studies of the same crystal indicating that the ground state of the staggered iron moments is not along the (0,1,0) direction, as previously reported from polycrystalline samples studies, but slightly rotated away from this axis.

DOI: 10.1103/PhysRevB.73.024410

PACS number(s): 75.25.+z, 75.30.Ds, 75.50.Ee

I. INTRODUCTION

Lithium-orthophosphates LiMPO_4 ($M=\text{Mn, Fe, Co, Ni}$) have attracted a renewed interest in recent years, both for their relatively high lithium-ionic conductivity that can potentially be applied in rechargeable battery technology¹ and for their intriguing magnetic properties, in particular, the strong magnetoelectric (ME) effect they exhibit.² In this regard, of particular importance is LiFePO_4 , as it has already been tested as a high-potential cathode in secondary Li-ion rechargeable battery.^{3–6} Like other members of the lithium-orthophosphates, LiFePO_4 is an insulator adopting the $Pnma$ space group.^{7,8} In this structure, the Fe^{2+} ion occupies the center of a slightly distorted MO_6 octahedron that shares oxygen anions with a PO_4 tetrahedron forming a closely packed oxygen framework. The Fe^{2+} ions ($S=2$) form corrugated layers that are stacked along the [100] crystallographic axis, as shown in Fig. 1(a). Nearest neighbors in the b - c plane are coupled magnetically by a relatively strong exchange interaction, J_1 through an Fe-O-Fe oxygen bond, whereas in-plane next-nearest-neighbors are coupled (J_2) via Fe-O-O-Fe (Ref. 9) [see Fig. 1(b) for definition of exchange couplings]. Interlayer magnetic coupling is mediated by a phosphate ion via an Fe-O-P-O-Fe bonding.¹⁰ Thus, the olivine family of LiMPO_4 exhibits highly anisotropic properties which are between those of two- (2D) and three-dimensional (3D) systems.^{11,12}

The magnetic properties of LiMPO_4 systems have been studied since the early 1960s.^{13–15} They all undergo an antiferromagnetic transition at low temperatures to a similar magnetic arrangement differing only in the orientation of the staggered spins. Nearest-neighbor (NN) spins in the b - c plane are antiparallel and the stacking along the a axis is such that ferromagnetic sheets perpendicular to the b axis are formed; nearest-neighbor sheets are antiparallel, giving rise to a (0,1,0) fundamental magnetic reflection that, depending on the direction of the magnetic moment, can be intense or extinct. Earlier neutron diffraction studies of polycrystalline samples showed that the magnetic space group of LiFePO_4 and LiCoPO_4 is $Pnma'$ with the spins oriented along the b

crystallographic direction (i.e., the (0,1,0) reflection is absent), and $Pnm'a$ magnetic space group for LiNiPO_4 and LiMnPO_4 with the spins aligned parallel to the c axis (i.e., strong intensity at the (0,1,0) reflection).^{11,12,15–18} Recent neutron diffraction measurements of single crystal LiCoPO_4 reported finite intensity at the (0,1,0) reflection, interpreted in terms of a ground state with a spin direction that is slightly rotated from the b axis.¹² Weak ferromagnetism has been reported for LiMnPO_4 ¹⁸ and LiNiPO_4 ¹⁹ at temperatures below T_N .

Recently, the magnetic structure and properties of lithium orthophosphates have been reexamined theoretically and experimentally.^{20,21} Rousse *et al.*²¹ reported neutron diffraction results from polycrystalline samples, confirming the collinear structure below $T_N=52$ K. Magnetic properties of LiFePO_4 investigated by Mössbauer spectroscopy and magnetization measurement determined that $T_N=50$ K.²² Theoretical estimations of the spin-exchange coupling by spin-dimer analysis, while neglecting the single-ion anisotropy, yield the following values: $J_1=1.08$ meV, $J_2=-0.4$ meV, and $J_\perp=-0.92$ meV.⁹ However, so far there has been no experimental determination of the exchange coupling among Fe^{2+} spins and of the single-ion anisotropy in LiFePO_4 , for comparison with the theoretical predictions. Knowledge of exchange couplings and single-ion anisotropy is also important for understanding the origin of the strong magnetoelectric (ME) effect in LiFePO_4 .¹³ All lithium orthophosphates exhibit a strong yet anomalous linear magnetoelectric (ME) effect with respect to the observed ME tensor components, α_{xy} , α_{yx} , for LiFePO_4 and LiCoPO_4 , and α_{xz} , α_{zx} for LiNiPO_4 , as expected with their respective antiferromagnetic point groups mmm' and $mm'm$.^{23–26} In particular, the ME effect measurements of LiFePO_4 as a function of temperature reveal a decrease of the ME coefficient along one direction $\alpha_{yx}(T)$ below a maximum close to T_N .^{23,24} Detailed determination of the magnetic structure using neutron diffraction from single crystals can shed light on the origin of these anomalies.

Herein, we report measurements of spin-wave dispersion curves of single-crystal LiFePO_4 by inelastic neutron scatter-

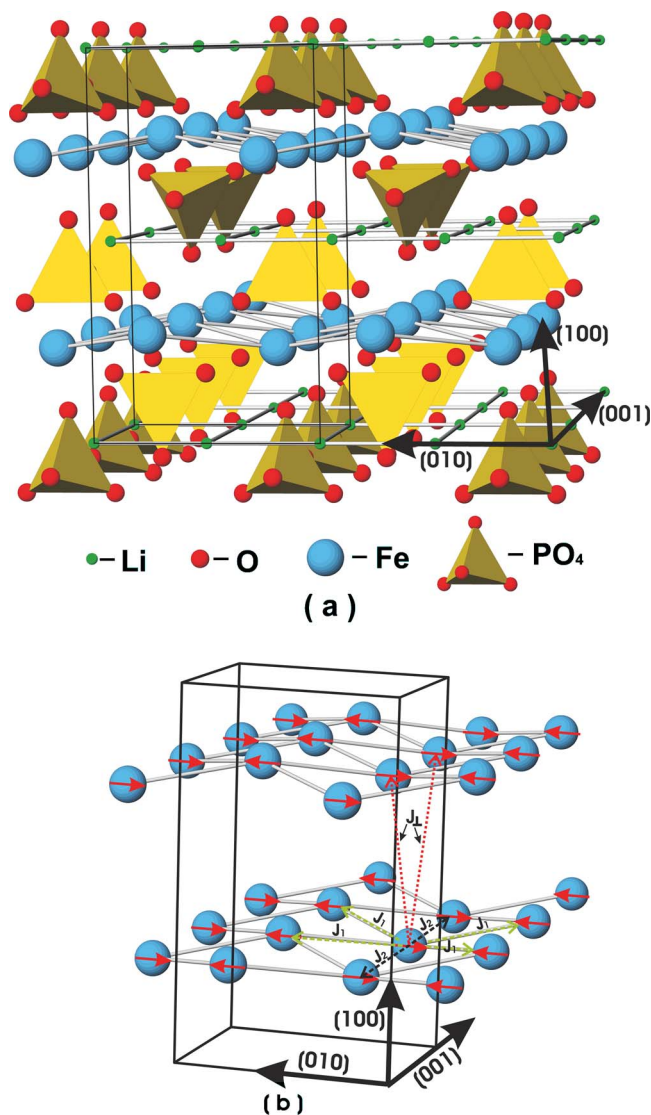


FIG. 1. (Color online) (a) Atomic structure of LiFePO₄. The Fe²⁺ ions form buckled layers stacked perpendicular to the [100] crystallographic direction. The ground state of LiFePO₄ is collinear antiferromagnetic with the average moment along *b* direction. (b) Spin arrangement of the two Fe²⁺ layers, the in-plane nearest and next-nearest-neighbor interactions J_1 and J_2 and interplane nearest-neighbor inaction J_{\perp} are labeled.

ing measurements. Spin-wave dispersion curves can provide the values of exchange interactions and the single-ion anisotropy. The measured dispersion curves were modeled using linear spin-wave theory by including the in-plane nearest-neighbors (NN) and next-nearest-neighbors (NNN) spin couplings, the interplane nearest-neighbor spin coupling, and the single-ion anisotropy. We have also employed single-crystal elastic neutron diffraction techniques to investigate whether there are subtle deviations from the previously reported magnetic structure determined from neutron diffraction measurements of polycrystalline samples.

II. EXPERIMENTAL DETAILS

LiFePO₄ single crystals were grown by standard flux growth technique (LiCl was used as the flux) from a sto-

ichiometric mixture of high purity FeCl₂ (99.999% Aldrich) and Li₃PO₄ (99.999% Aldrich).²⁷ The grown single crystals have a dark greenish color. The composition and structure were confirmed by carrying out Rietveld analysis of the x-ray powder diffraction (XRD) data, using the GSAS software package.²⁸ No extra peaks from impurities were detected in the XRD pattern. Powder, for the XRD, was produced by crushing typical isolated single crystals from the melt. The lattice parameters yielded from the refinement ($a = 10.337$ Å, $b = 6.011$ Å, and $c = 4.695$ Å) are in good agreement with literature values.^{15,20,21}

Neutron scattering measurements were carried out on the HB1A triple-axis spectrometer at the high flux isotope reactor at Oak Ridge National Laboratory. A monochromatic neutron beam of wavelength $\lambda = 2.366$ Å (14.6125 meV, $k_o = 2\pi/\lambda = 2.656$ Å⁻¹) was selected by a double monochromator system, using the (0,0,2) Bragg reflection of highly oriented pyrolytic graphite (HOPG) crystals. HOPG crystal was also used as analyzer for both the elastic and the inelastic studies. The $\lambda/2$ component in the beam was removed by two HOPG filters located before and after the second monochromator. The collimating configuration 40'40' sample 34'68' was used throughout the experiments. Temperature measurements and control were achieved by a Conductus LTC-20 using Lake Shore silicon-diode temperature sensors. An irregular shaped single crystal (weight ~ 0.4 g) was folded in aluminum foil and mounted on a thin aluminum post. It was then sealed in an aluminum can under helium atmosphere and loaded onto the tip of a closed-cycle helium refrigerator (Displex). Two temperature sensors were mounted on the cold tip of the Displex and on the sample can. The temperature was controlled using the cold-tip sensor. The temperature difference between the two sensors was about 0.2 K over the temperature range investigated.

III. RESULTS AND DISCUSSION

A. Elastic neutron scattering

The LiFePO₄ crystal was oriented such that the *a-b* plane coincided with the horizontal scattering plane of the spectrometer. The elastic measurements confirmed that the magnetic structure of LiFePO₄ is antiferromagnetic with the main direction of the moment oriented along the *b* axis. However, contrary to the previous neutron diffraction experiments performed on powder samples, we have detected the presence of the (0,1,0) reflection. The intensity of this peak is relatively weak but its intensity follows a similar temperature dependence as that of a stronger magnetic peak (2,1,0) (see Fig. 2). It is worth noting that the (0,1,0) peak is forbidden by the symmetry of the $Pnma'$ magnetic space group previously proposed to describe the spin arrangement in LiFePO₄.^{15,20} In the $Pnma$ crystal symmetry, the point group of the Fe 4*c* site is m_y and the only allowable magnetic point groups are, therefore, m_y with the Fe magnetic moments along the *b* axis [perpendicular to the mirror (0,1,0) plane] and m'_y with the magnetic moment lying in the mirror (0,1,0) plane. The magnetic contribution to the (0,1,0) peak indicates that the ordered moment is not strictly oriented along the *b* axis and a small component perpendicular to this axis is

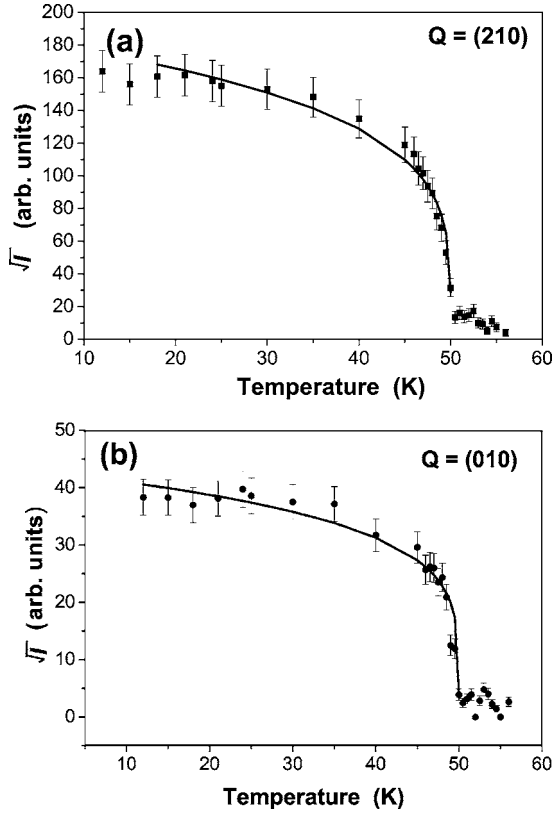


FIG. 2. Temperature dependence of the square root of the normalized integrated intensity at two reflection peaks (2,1,0) (a) and (0,1,0) (b). The transition temperature obtained from the fitting is $T_N = 50 \pm 0.5$ K and the critical exponent $\beta = 0.27 \pm 0.03$.

present. This implies a lowering of the symmetry of the magnetic space group where both magnetic components (along and perpendicular to the b axis) are allowed. From the intensity ratio of the two reflections $I(0,1,0)/I(2,1,0)$ at low temperatures, we can estimate the angle of the staggered moment with respect to the b axis by using the following relation:

$$\frac{F_{(010)} \sin(\alpha_{(010)})}{F_{(210)} \sin(\alpha_{(210)})} = \sqrt{\frac{I_{(010)} \sin(2\theta_{(210)}) f_{(210)}}{I_{(210)} \sin(2\theta_{(010)}) f_{(010)}}}, \quad (1)$$

where $F_{(210)}$ and $F_{(010)}$ are the magnetic structure factors of peaks (2,1,0) and (0,1,0), $\alpha_{(210)}$, $\alpha_{(010)}$ are the angles between the scattering vector of reflections (210), (010) and the magnetic moment, and f_i are the corresponding form factors.¹² Using $f_{(210)}/f_{(010)} \approx 0.85$, we estimate the moments are rotated by 7.5 ± 0.5 deg toward the c axis or 3 ± 0.5 deg toward the a axis. The ratio between the magnetic and nuclear contributions to the peak intensities of reflections (I_{mag}/I_{nuc}) can be used to determine the average magnetic moment, μ , from

$$\mu = \sqrt{\frac{I_{mag} |F_{nuc}|^2}{I_{nuc} |F_{mag}|^2 f^2(Q) \sin^2 \alpha}}, \quad (2)$$

where, for the reflection in question, F_{nuc} and F_{mag} are the nuclear and magnetic structure factors, I_{nuc} and I_{mag} are the nuclear and magnetic intensities, and $f(Q)$ is the magnetic

form factor of Fe^{2+} at momentum transfer $Q = 2k_0 \sin \theta$. I_{mag} can be calculated from the peak intensity difference at temperatures above and below T_N . Using the peak intensities of (2,1,0) at 300 K and 10 K to calculate the I_{mag} and I_{nuc} , and using $f_{(210)} = 0.85$, the calculated average magnetic moment μ for Fe is $3.93 \pm 0.05 \mu_B$, which is very close to the values of $3.99 \mu_B$ and $3.8 \mu_B$ obtained in Refs. 29 and 30.

To determine the temperature dependence of the order parameter, the (0,1,0) and (2,1,0) reflections were monitored as a function of temperature in the range between 10 and 60 K. Figures 2(a) and 2(b) show the square root of the integrated intensity (\sqrt{I}) versus temperature. The \sqrt{I} quantity is proportional to the antiferromagnetic staggered magnetization, i.e., the order parameter. It was fitted to the following power law function over a wide range of temperatures below T_N ,

$$\sqrt{I} \propto M^{\dagger} = M_0^{\dagger} t^{\beta}, \quad (3)$$

where M_0^{\dagger} is the sublattice magnetization at $T=0$ K, $t = (1 - T/T_N)$ is the reduced temperature. For the two magnetic peaks (0,1,0) and (2,1,0) the obtained transition temperatures are the same, $T_N = 50 \pm 0.5$ K and the exponent β is 0.27 ± 0.03 . The transition temperature is very close to the values reported in the literature 50 ± 2 K.^{15,20,22} It should be noted that the value of the phenomenological exponent β extracted by using Eq. (3) over a wide range of temperatures is not the same as the theoretical critical exponent which is strictly defined in the vicinity of a critical temperature (for $|t| \ll 1$). And therefore, the fact that β is just slightly smaller than the theoretical critical exponent for the 3D cubic Ising model ($\beta = 0.32$)³¹ does not necessarily imply that the magnetic system is 3D in character. Similar values of β using Eq. (3) to phenomenologically describe the staggered magnetization were reported for other layered systems that exhibit 2D magnetism. For instance, for the 2D spin $\frac{1}{2}$ model system $\text{Sr}_2\text{Cl}_2\text{CuO}_2$ the interplane coupling J_{\perp} is much smaller than the in-plane coupling J_{\parallel} ($J_{\perp} \ll J_{\parallel}$) while $\beta = 0.39$.³² As shown below, the spin-wave analysis of LiFePO_4 yields $J_{\perp} \ll J_{\parallel}$, and therefore the magnetic system in LiFePO_4 can be classified as a quasi-2D system. In this regard, the temperature dependent backgroundlike scattering above T_N extending to ~ 60 K indicates some kind of critical scattering due to short-range order and/or due to a dimensionality crossover.

B. Inelastic neutron scattering

The spin-wave excitations were measured at 10 K along the $(\xi, 1, 0)$ and $(0, 1 + \xi, 0)$ reciprocal space directions, for energy transfers (energy loss mode) ranging from 1 to 8.5 meV. As illustrated in Figs. 3(a)–3(c), well-defined dispersive magnetic modes of resolution-limited energy width were observed at all wave vectors. A typical energy scan at constant- Q scan, performed at the zone center (0,1,0), is shown in Fig. 3(a), indicating a single excitation at an energy transfer of 5.86 ± 0.04 meV. The increase in intensity at energy transfer below approximately 1 meV is due to the quasielastic scattering from the newly observed (0,1,0) magnetic Bragg peak. Above the transition temperature ($T_N = 50$ K), at approximately 55 K, the inelastic peak at

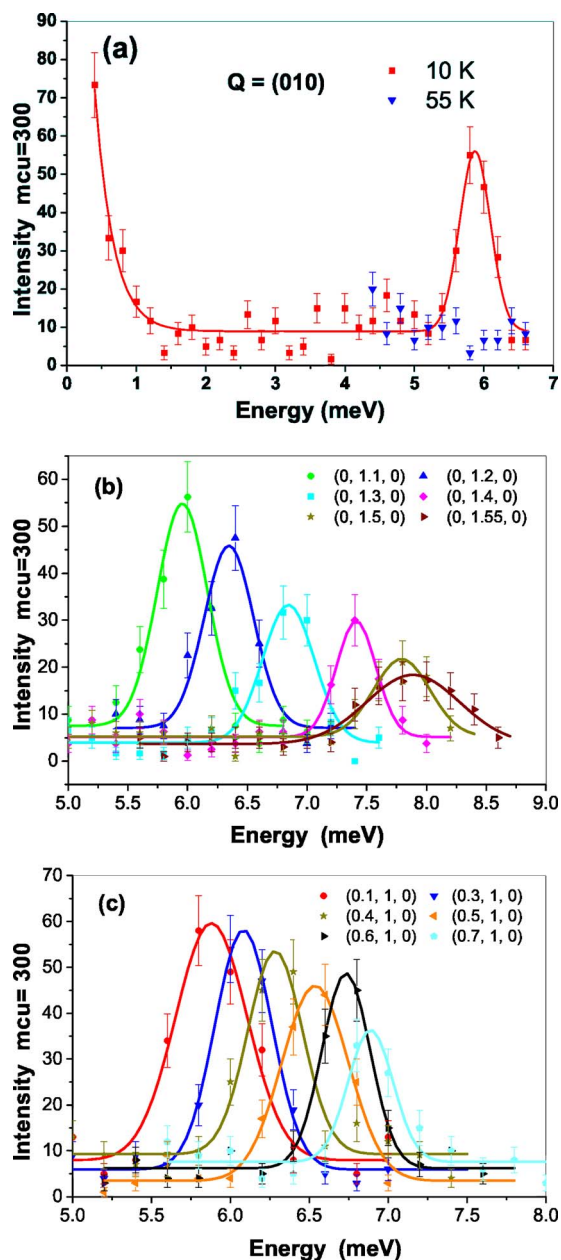


FIG. 3. (Color online) (a) Neutron scattering intensity as a function of the energy transfer E at $(0,1,0)$ peak at 10 K and 55 K. (b) Constant- Q scans taken at 10 K, at different wave vectors $(0, 1 + \xi, 0)$ and (c) Constant- Q scans at $(\xi, 1, 0)$.

5.86 meV disappears, confirming its magnetic origin. Such an energy gap in the dispersion curve is usually driven by single-ion anisotropy. A similar energy gap of 2 meV at 2 K, was also observed in the LiNiPO_4 , and it was found to decrease with increasing the temperature.³³ In the case of LiFePO_4 , measurements performed at different temperatures indicate that the energy gap is temperature independent. The inelastic scattering signal measured at different constant wave vectors ξ along the $(1,0,0)$ and $(0,1,0)$ reciprocal-space directions, at 10 K, are shown in Figs. 3(b) and 3(c). The data were fitted to Gaussian functions [solid line in Figs. 3(a)–3(c)] where the background was assumed to be constant.

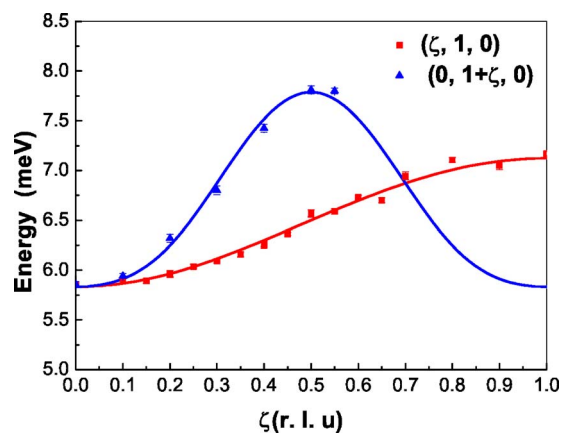


FIG. 4. (Color online) Spin-wave dispersion curves along the b^* and a^* reciprocal-space directions. Solid lines are fits obtained from linear spin-wave theory using Eq. (5).

The spin-wave dispersion branches deduced from these fits, for both b^* and a^* reciprocal-space directions, are plotted in Fig. 4. It is shown that the dispersion curves monotonically increase in energy with ξ , and that the spin waves propagating in the plane along the $(0,1,0)$ direction have higher frequencies than those propagating transversally along the $(1,0,0)$. Qualitatively, this behavior reflects the anisotropy in the strength of exchange couplings in the system; as expected, the in-plane exchange couplings are much stronger than those between planes.

To construct a Hamiltonian for the spin system, we recall that in the LiMPO_4 olivine family the in-plane superexchange or super-superexchange interactions between nearest and next-nearest neighboring Fe^{2+} ions (J_1 and J_2) are expected to be much stronger than that between the nearest interplane neighbors (J_\perp).^{10,34} For simplicity, we assume that the exchange interactions are isotropic, Heisenberg-like, so anisotropies in the different components of the couplings are averaged. Therefore, we propose the following Hamiltonian:

$$\mathcal{H} = -J_1 \sum_{i,\delta} (S_i S_{i+\delta}) - J_2 \sum_{i,\xi} (S_i S_{i+\xi}) - J_\perp \sum_{i,\delta_\perp} (S_i S_{\delta_\perp}) + D \sum_i (S_i^z)^2, \quad (4)$$

where J_1 and J_2 are the in-plane NN and NNN coupling constants, respectively, and J_\perp is the interplane NN coupling constant. The illustrations of J_1 , J_2 , and J_\perp are shown in Fig. 1(b). D is the single-ion anisotropy constant quantifying the tendency of the spins to align along the easy axis (the S^z component is defined to be along the direction of the moment at the ground state, b^*). The Ising-like ground state of the system is believed to be invoked by the single-ion anisotropy term which comes about from crystal field effects and spin-orbit coupling.³⁵ Using the antiferromagnetic spin-wave theory,^{36,37} the lattice with N sites was divided into two sublattices A and B , where nearest neighbors of an Fe^{2+} site in one sublattice are all sites in the other sublattice. The next-nearest neighbors of an Fe^{2+} site are in the same sublattice. The magnon dispersion curves were calculated using the

Holstein-Primakoff spin operator transformation to linear approximation (i.e., linear spin-wave theory³⁸). The resulting spin-wave dispersion is given by

$$\hbar\omega = \sqrt{A^2 - F^2}, \quad (5)$$

where $A = (2J_1ZS - 2J_2ZS - 2J_{\perp}ZS + 2J_2ZS\gamma_{3N} + 2J_{\perp}ZS\gamma_{\perp} + 2DS)$ and $F = 2J_1ZS\gamma_{2N}$, in which Z is the number of the nearest neighbors $Z=4$, $S=2$ for Fe^{2+} . γ_{2N} , γ_{3N} , and γ_{\perp} are calculated using the following equation:

$$\gamma_{(2N,3N,\perp)} = \frac{1}{Z} \sum_i e^{i\mathbf{Q}\cdot\mathbf{r}}, \quad (6)$$

where $\mathbf{r} = (\delta, \xi, \delta_{\perp})$ are the components of vectors to the intraplane nearest-, next-nearest neighbors, and to the interplane nearest neighbor. We get

$$\gamma_{2N} = \cos(\pi k_y) \cos(\pi k_z), \quad (7)$$

$$\gamma_{3N} = \frac{1}{2} [\cos(2\pi k_y) + \cos(2\pi k_z)], \quad (8)$$

$$\gamma_{\perp} = \cos(\pi k_x) \cos(\pi k_y). \quad (9)$$

The experimental data along the $(0, 1 + \delta, 0)$ and $(\delta, 1, 0)$ directions in Fig. 4 were fitted to Eq. (5) yielding the following values: $J_1 = -0.662 \pm 0.02$ meV, $J_2 = -0.27 \pm 0.02$ meV, $J_{\perp} = 0.021 \pm 0.001$ meV, and $D = -0.37 \pm 0.01$ meV.

The in-plane nearest- and next-nearest-neighbor coupling constants quantitatively agree with theoretical calculations,⁹ $J_1 = -1.08$ meV and $J_2 = -0.4$ meV.⁹ The two spin couplings, $J_1 < 0$ and $J_2 < 0$, compete oppositely over the alignment of in-plane NNN spins; whereas J_1 leads to parallel alignment of NNN spins J_2 favors their antiparallel alignment. Such competing interactions can lead to incommensurate phases³⁹ which were not found in this system. However, incommensurate phases have been reported for the isostructural LiNiPO_4 .²⁶ The interplane coupling $J_{\perp} = 0.021$ meV (ferromagnetic coupling according to our notation) determined in

this study is significantly different than the theoretical one $J_{\perp} = -0.92$ meV,⁹ which predicts antiferromagnetic coupling among interplane NN. Our result for J_{\perp} is consistent with the magnetic structure shown in Fig. 1, with parallel interplane NN spins. Furthermore, the small ratio $J_1/J_{\perp} \approx 30$ is consistent with the layered nature of LiFePO_4 , and also reflects the fact that the interplane coupling between NN spins is very weak as it is mediated via a phosphate group.¹⁰ It should be noted that single-ion anisotropy was not considered in the theoretical calculations.⁹

To summarize, we have measured spin-wave dispersions and determined spin-exchange couplings in LiFePO_4 . Our results show that although there are competing interactions between NN and NNN spins in LiFePO_4 , they do not lead to more complicated, incommensurate, or noncolinear magnetic structures. This is in contrast to the observation of incommensurate magnetic phases in LiNiPO_4 .²⁶ These competing interactions may explain the weak ferromagnetism in LiMPO_4 systems observed by other techniques¹⁸ (the neutron scattering techniques we used did not detect such weak ferromagnetism in LiFePO_4 , possibly due to the lack of sensitivity). They may also be related to the observation, in this study, that the staggered magnetic moment is not aligned along a principal direction. From the gap in the spin-wave dispersion curve, we have been able to extract the single-ion anisotropy in LiFePO_4 using linear spin-wave theory.

ACKNOWLEDGMENTS

We thank R. J. McQueeney, S. Chang, and J. Q. Yan at Ames Laboratory for the helpful discussions. This work was supported (in part) under the auspices of the United States Department of Energy. The HFIR Center for Neutron Scattering is a national user facility funded by the United States Department of Energy, Office of Basic Energy Sciences, Materials Science, under Contract No. DE-AC05-00OR22725 with UT-Battelle, LLC. The work was supported by the Department of Energy, Office of Basic Energy Sciences under Contract No. W-7405-Eng-82.

*Electronic mail: jiy@ameslab.gov

†Electronic mail: vaknin@ameslab.gov

¹J.-M. Tarascon and M. Armand, *Nat. Mater.* **414**, 359 (2001).

²M. Fiebig, *J. Phys. D* **38**, R123 (2005).

³A. K. Padhi, K. S. Nanjundaswamy, and J. B. Goodenough, *J. Electrochem. Soc.* **144**, 1188 (1997).

⁴S. Y. Chung, J. T. Bloking, and Y. M. Chiang, *Nat. Mater.* **1**, 123 (2002).

⁵P. S. Herle, B. Ellis, N. Coombs, and A. F. Nazar, *Nat. Mater.* **3**, 147 (2004).

⁶C. Delacourt, P. Poizot, J. M. Tarascon, and C. Masquelier, *Nat. Mater.* **4**, 254 (2005).

⁷S. Geller and J. L. Easson, *Acta Crystallogr.* **18**, 258 (1960).

⁸H. D. Megaw, *Crystal Structures—A Working Approach* (Saunders, Philadelphia, 1973), p. 249.

⁹D. Dai, M. H. Whangbo, H. J. Koo, X. Rocquefelte, S. Jobic, and

A. Villesuzanne, *Inorg. Chem.* **44**, 2407 (2005).

¹⁰J. M. Mays, *Phys. Rev.* **131**, 38 (1963).

¹¹D. Vaknin, J. L. Zarestky, J. E. Ostenson, B. C. Chakoumakos, A. Goñi, P. Pagliuso, T. Rojo, and G. E. Barberis, *Phys. Rev. B* **60**, 1100 (1999).

¹²D. Vaknin, J. L. Zarestky, L. L. Miller, J.-P. Rivera, and H. Schmid, *Phys. Rev. B* **65**, 224414 (2002).

¹³M. Mercier, J. Gareyte, E. F. Bertaut, and C. R. Seances, *C. R. Seances Acad. Sci., Ser. B* **264**, 979 (1967).

¹⁴R. P. Santoro, D. J. Segal, and R. E. Newnham, *J. Phys. Chem. Solids* **27**, 1192 (1966).

¹⁵R. P. Santoro and R. E. Newnham, *Acta Crystallogr.* **22**, 344 (1967).

¹⁶A. Goñi, L. Lezama, G. E. Barberis, J. L. Pizarro, M. I. Arriortua, and T. Rojo, *J. Magn. Magn. Mater.* **164**, 251 (1996).

¹⁷D. Arçon, A. Zorko, R. Dominko, and Z. Jaglicic, *J. Phys. Chem.*

- Solids **16**, 5531 (2004).
- ¹⁸Y. Kharchenko, N. Kharchenko, M. Baran, and R. Szymczak, *Low Temp. Phys.* **29**, 579 (2003).
- ¹⁹D. Arčon, A. Zorko, P. Cevc, R. Dominiko, M. Bele, J. Jamnik, Z. Jaglicic, and I. Golosocsky, *J. Phys. Chem. Solids* **65**, 1773 (2004).
- ²⁰V. A. Streltsov, E. L. Belokoneva, V. G. Tsirelson, and N. K. Hansen, *Acta Crystallogr.* **B49**, 147 (1993).
- ²¹G. Rouse, J. R. Carvajal, S. Patoux, and C. Masquelier, *Chem. Mater.* **15**, 4082 (2003).
- ²²Luo Zhi, Di Nai-Li, Kou Zhi-Qi, Cheng Zhao-Hua, Liu Li-Jun, Chen Li-Quan, and Huang Xue-Jie, *Chin. Phys.* **13**, 2158 (2004).
- ²³M. Mercier and P. Bauer, *Acad. Sci., Paris, C. R.* **267**, 465 (1968).
- ²⁴M. Mercier, *Rev. Gen. Electr.* **80**, 143 (1971).
- ²⁵J.-P. Rivera, *Ferroelectrics* **161**, 147 (1994).
- ²⁶D. Vaknin, J. L. Zarestky, J.-P. Rivera, and H. Schmid, *Phys. Rev. Lett.* **92**, 207201 (2004).
- ²⁷V. I. Fomin, V. P. Genezdilov, V. S. Kurnosov, A. V. Peschanskii, A. V. Yeremenko, H. Schmid, J.-P. Rivera, and S. Gentil, *Low Temp. Phys.* **28**, 203 (2002).
- ²⁸A. C. Larson, R. B. Von Dreele, and M. Lujan Jr., *Computer Code GSAS, Generalized Structure Analysis System* (Neutron Scattering Center, Los Alamos National Laboratory, 1990).
- ²⁹Y. N. Xu, S. Y. Chung, J. T. Bloking, Y. M. Chiang, and W. Y. Ching, *Electrochem. Solid-State Lett.* **7**, A131 (2004).
- ³⁰A. Yamada, S. C. Chung, and K. Hinokuma, *J. Electrochem. Soc.* **148**, A224 (2001).
- ³¹M. F. Collins, *Magnetic Critical Scattering* (Oxford University Press, New York, 1989), p. 29.
- ³²D. Vaknin, S. K. Sinha, C. Stassis, L. L. Miller, and D. C. Johnston, *Phys. Rev. B* **41**, 1926 (1990); D. Vaknin, L. L. Miller, J. L. Zarestky, and D. C. Johnston, *Physica C* **274**, 331 (1997).
- ³³J. Li, D. Vaknin, and J. L. Zarestky (unpublished).
- ³⁴S. Shi, C. Y. Quyang, Z. H. Xiong, L. J. Liu, Z. X. Wang, H. Li, D. S. Wang, L. Q. Chen, and X. J. Huan, *Phys. Rev. B* **71**, 144404 (2005).
- ³⁵L. J. de Jongh, *Magnetic Properties of Layered Transition Metal Compounds* (Kluwer Academic, Dordrecht, 1990), p. 1.
- ³⁶P. W. Anderson, *Phys. Rev.* **86**, 694 (1952).
- ³⁷R. Kubo, *Phys. Rev.* **87**, 568 (1952).
- ³⁸G. L. Squires, *Introduction to the Theory of Thermal Neutron Scattering* (Cambridge University Press, New York, 1978), p. 156.
- ³⁹P. Bak, *Rep. Prog. Phys.* **45**, 687 (1982).